EUROPEAN ORGANIZATION FOR NUCLEAR RESEARCH

CERN/ISRC/73-21
2 July 1973

STUDIES OF QUASI-TWO-BODY PROCESSES AT ISR ENERGIES

CERN: R. Kofler and F. Muller

Northwestern University: M. Block, B. Gobbi, D. Miller, J. Rosen and R. Ruchti

Orsay: A. Orkin-Lecourtois

ABSTRACT

The physics proposed is to study the quasi-two-body reactions

$$pp \to \Delta^{++}\Delta^{0} \quad (1)$$
$$pp \to \Delta^{++}n \quad (2)$$
$$pp \to \Delta^{+}\Delta^{+} \quad (3)$$
$$pp \to \Delta^{+}p \quad (4)$$
$$pp \to N^{*+}N^{*+} \quad (5)$$
$$pp \to N^{*+}p \; . \quad (6)$$

The first two charge exchange reactions study $\rho + A_2$ exchange, which at the upper end of the ISR energy domain should dominate over pion exchange. Reactions (3) and (4) have dominant Coulomb contributions. Reactions (5) and (6) study low mass double diffraction dissociation and single diffraction dissociation, respectively, and are necessarily experimentally intertwined with (3) and (4). We propose to use the R603 apparatus in a compatible mode, i.e. without disturbing the physics scheduled for it, by adding to the detector capability.

1. INTRODUCTION

This proposal is to study quasi-two-body reactions at the ISR. For clarity, the physics is divided into two parts. Section 2.1 deals with charge exchange processes

$$pp \to \Delta^{++}\Delta^{0} \tag{1}$$

$$pp \to \Delta^{++}n \ , \tag{2}$$

where we detect the decay modes of the $\Delta(1238)$ MeV, $\Delta^{++} \to p\pi^{+}$ and $\Delta^{0} \to p\pi^{-}$.

In Section 2.2, we consider the reactions

$$pp \to \Delta^{+}\Delta^{+} \tag{3}$$

$$pp \to \Delta^{+}p \ , \tag{4}$$

along with the low mass spectrum of the double and single diffractive dissociation channels

$$pp \to N^{*+}N^{*+} \tag{5}$$

$$pp \to N^{*+}p \ , \tag{6}$$

respectively.

We will later emphasize the importance of Coulomb processes (one-photon exchange) that also contribute to reactions (3) and (4).

Throughout the discussion we will stress the unique character and advantages of measuring these two-body channels [reactions (1)-(4)] in the VHE (Very High Energy) limit, an energy domain now accessible at the ISR.

Section 2 gives a brief description of the physics goals, and attempts to summarize the details of these reactions which are more extensively discussed in the Appendix, as well as to outline the experimental configurations required.

Section 3 is a summary. Rate estimates at 1500 GeV are presented, as well as a brief discussion of the expected energy dependence of the reactions. The compatibility of the experiment with the present R603 apparatus is stressed, and running time for the experiment is requested.

2. PHYSICS GOALS AND EXPERIMENTAL ARRANGEMENT

2.1 Charge exchange processes

For orientation purposes, let us consider the three distinct energy regions, in which the charge-exchange reactions (1) and (2) are expected to have quite different cross-sectional behaviors.

LHE -- Low High Energies -- by this, we mean the energy region from 5-30 GeV. Here, experimental data indicate that pion exchange dominates in reactions (1) and (2). The cross-section drops as $\sim 1/p^2$, with p being the lab. momentum.

HE -- High Energies -- perhaps from 100 to 300 GeV. In the HE region, pion exchange is expected to compete now with $\rho + A_2$ exchange, with both being of comparable importance.

VHE -- Very High Energy -- the ISR energy region. At VHE, the pion contribution has greatly diminished in importance, whereas the $\rho + A_2$ contribution (having a much slower energy dependence) should dominate the reaction. The ISR energy range allows us to investigate this for the first time.

Kane, Drummond and Block[1] have estimated cross-sections for reactions (1) and (2) in the VHE region, based on simplifying assumptions which are discussed in Appendix 1, where the theoretical situation is dealt with in some detail. The principal conclusions and results are repeated below.

2.1.1 $pp \to \Delta^{++}n$

We have as measurables $(d\sigma/dt)(t,s)$ and the angular decay distribution function $W(\theta,\phi)$, also as a function of s,t. We expect this reaction to be dominated by $\rho + A_2$ exchange at ISR upper energies, i.e. to be the first example where a lower-lying trajectory takes over a higher one. At 1500 GeV, we estimate a total cross-section (for $\rho + A_2$ only) of ~ 0.2 μb, in contrast to the pion contribution, estimated by a $1/p^2$ contribution, of 0.025 μb. Thus we expect to see an order of magnitude increase in the total rate $pp \to \Delta^{++}n$. The t-structure, given by the solid curve in Fig. A1a, suggests a gentle peak in the neighbourhood of $-t \approx 0.10$ GeV^2. The angular distribution will allow us to measure the density matrix elements ρ_{11}, ρ_{33}, ρ_{31}, and ρ_{3-1}, and thus to measure the effects of absorption

on the pole terms. If the experimental situation is as simple as the proposed model, a detailed amplitude separation is possible. However, the main qualitative feature of the experiment is the Regge expectation that the observed cross-section will be much larger ($\sim$ 10 times at 1500 GeV) than the extrapolated results from low energy, indicating that as we pass from HLE to VHE, the lower-lying trajectories will eventually dominate.

We propose to measure $pp \to \Delta^{++}n$ by adding detectors to the present R603 set-up, i.e. by putting a calorimeter (hadrometer) on the opposite arm, as sketched in Fig. 1. The calorimeter is the one referred to in the documents CERN/ISRC/69-19 Add. 18 and CERN/ISRC/72-3 Add. 3. In order to suppress π^0 events, we would add γ-ray detectors to this arm, operating in anticoincidence. The trigger would be two charged particles in the spectrometer, a veto over all large angles, a veto in the γ-ray counters, i.e. no neutrals on the other side, and a large energy deposition in the calorimeter. The neutron energy and a rough angle determination are made in the calorimeter, and the $\Delta^{++} \to p\pi^+$ is detected in the magnetic spectrometer. The acceptance of the device is basically limited by the magnetic spectrometer. Detailed Monte Carlo acceptance calculations, using the assumed theoretical angular decay distributions of the Δ^{++}, are being carried out. Preliminary estimates of the acceptance range between 10 and 30%. Using the conservative figure of 10%, we estimate the counting rate by dividing the estimated cross-section by 2 to allow for the fact that Δ^{++} is only detected in one arm. We assume a luminosity of 4×10^{30} per cm^2 sec, and get

$$R(\Delta^{++}n) = 0.10 \times (2 \times 10^{-31}) \times \frac{1}{2} \times 4 \times 10^{30}/\text{sec} \approx 150 \text{ counts/hour} ,$$

at a lab. equivalent energy of 1500 GeV. The cross-section is higher at the lower energies.

2.1.2 $\underline{pp \to \Delta^{++}\Delta^0}$

We again measure $d\sigma/dt$ as a function of s and t. The experimental situation is richer for this reaction, since we have the joint angular distribution $W(\theta_1,\phi_1; \theta_2,\phi_2)$ of both Δ's to measure, giving us more information than the single decay distribution of reaction (1). The theoretical situation in the model proposed in Appendix 1 is even simpler for

$pp \to \Delta^{++}\Delta^0$ than for $pp \to \Delta^{++}n$, since in this case we have but two amplitudes, and the double decay allows a complete amplitude analysis as a function of t and s. We again expect the reaction to test Reggeism, i.e. at VHE, it should be dominated by $\rho + A_2$ exchange. The theoretical cross-section $d\sigma/dt$ is shown at 1500 GeV as the solid curve in Fig. A1b. We see a drop in t, with a minimum at ~ 0.05, followed by a gradual maximum and eventual slow drop. The integrated cross-section is ~ 0.1 μb, whereas the extrapolated $(1/p^2)$ cross-section from low energies gives ~ 0.020 μb.

To detect this reaction with the basic R603 configuration, we have two modes. In mode 1 we detect $\Delta^{++} \to p\pi^+$ in the magnetic spectrometer, and the decay $\Delta^0 \to p\pi^-$ in the other arm, with the proton energy and rough angle being measured in the calorimeter, and the pion and proton angles in the MWPC. We estimate that the mass resolution of the Δ^0 will be ~ 35 MeV, sufficient for identification. In mode 2 we detect the $\Delta^{++} \to p\pi^+$ in the calorimeter -- MWPC system, and the $\Delta^0 \to p\pi^-$ in the magnetic spectrometer. In addition to doubling the rate, this gives us an experimental versatility in being able to check, from symmetry, on acceptance, mass resolution, etc. Again, using the figure of $4 \times 10^{30}/cm^2$ sec for the luminosity, the 10% acceptance, a cross-section of 0.1 μb at 1500 GeV, and a factor of $\frac{1}{3}$ to allow for detection of the $\pi^- p$ decay of the Δ^0, we get

$$R_{\Delta^{++}\Delta^0} = 0.1 \times \frac{1}{3} \times (1 \times 10^{-31}) \times 4 \times 10^{30}/\text{sec} \approx 50 \text{ counts/hour} .$$

An alternate detection scheme of the Δ^0, i.e. $\Delta^0 \to n\pi^0$, is to use the γ-ray detectors to measure the π^0 energy and direction, and the calorimeter to measure the neutron energy and rough angle. If this gives sufficient resolution, we will increase the counting rate by ≈ 50 counts per hour by detecting $\Delta^0 \to n\pi^0$.

The trigger for the charged particle modes will be two charged particles, both into the spectrometer and the calorimeter --- MWPC set-up, with a minimum energy deposition in the calorimeter. Of course, vetoes will be required at all other angles.

For the decay $\Delta^0 \to n\pi^0$, we require no charged particles entering the calorimeter -- MWPC set-up, large energy deposition in the calorimeter, a signal in the γ-ray detectors, and vetoes elsewhere.

2.2 Non-charge exchange reactions

2.2.1 $pp \to \Delta^+ p$ and $pp \to N^{*+} p$

As shown in Fig. A2a, for $-t \lesssim 0.4$, the reaction $pp \to \Delta^+ p$ is dominated by Coulomb processes (one-photon exchange), which have a t-behavior which is essentially a spike at $t \approx 3t_{min}$, with a width $\sim t_{min}$. The integrated Coulomb cross-section, at 1500 GeV, from $t_{min} \leq -t \leq 0.0009$, is ~ 5 μb. Of course, all one will be able to detect is the integrated spike of this cross-section. The possibility of resolving this very, very narrow t-distribution is beyond any present experimental resolution capability. By plotting the t-distribution and observing the forward spike, we should effectively be able to separate the Δ's from any contribution of low mass N^*'s produced in single diffraction dissociation. Because the $\Delta^+ \to p\pi^0$ two-thirds of the time, whereas the $T = \frac{1}{2}$ diffractive N^*'s decay into $p\pi^0$ only one-third of the time, the ratio of Δ^+/N^{*+} via the decay mode $p\pi^0$ is four times better than this ratio if we detected $n\pi^+$. Clearly, however, in order to do this experiment, we must also measure the mass spectrum of low-mass diffractively produced N^{*+}, at the same time we attempt to measure the Δ^+. The theoretical situation changes for $t \gtrsim 0.4$. There, the nuclear forces dominate, and the ratio of $\sigma(pp \to \Delta^+ p) = \frac{1}{3}\,\sigma(pp \to \Delta^{++} n)$. This will furnish us with a calibrator to test our ability to extract Δ^+ from the possibly large background of low mass diffractive N^{*+}.

We propose to detect $\Delta^+ \to p\pi^0$ by having the proton traverse the calorimeter, and detect the proton angle in the MWPC. The π^0 would be detected in the γ-ray counters. For this detection mode, the required trigger would be 0 or 1 charged particle traversing the magnetic spectrometer, one charged particle on the other arm, a signal in the γ-ray counters, and a large energy deposition in the calorimeter. We also add to this trigger requirement a veto from a π^0 detector located behind the magnet spectrometer. We can also detect in the reverse mode, i.e. have the proton from the Δ^+ in the spectrometer, detect the π^0 behind the magnet spectrometer, and have the produced proton go into the calorimeter. Again there may well be experimental advantages in calibrating our system by these very asymmetric methods of measuring symmetric reactions.

The paper of Nicot and Salin[2] estimates that the total cross-section of $\Delta^+ p$ is $\sim$ 10 μb from the Coulomb contribution, at 1500 GeV. The large ratio of Coulomb to strong cross-section is qualitatively understood because of two effects:

i) the total nuclear cross-section drops with increasing energy;

ii) the Coulomb cross-section is singular in t, going as $\sim 1/t$, and the total cross-section grows logarithmically with energy.

This gives us, crudely, an estimated rate of

$$R_{\Delta^+ p} = 0.1 \times \frac{2}{3} \times 10^{-29} \times 4 \times 10^{30}/\text{sec} \approx 10{,}000 \text{ counts/hour} .$$

The major problem is the low efficiency for forward Δ^+ decays, where, due to their small opening angle, we lose a large fraction of the protons because they go through the septum. At larger t, this problem is no longer serious. The low t data, since it has a known cross-section, might well serve as a Coulomb calibrator of the accelerator, and can be compared to the Van der Meer method at the same energy. At larger t we will be investigating the mass spectrum of single diffractively dissociated $N^{*+} \rightarrow p\pi^0$, as well as Δ^+ produced by $\rho + A_2$ exchange.

2.2.2 $pp \rightarrow \Delta^+\Delta^+$ and $pp \rightarrow N^{*+}N^{*+}$

The situation for $pp \rightarrow \Delta^+\Delta^+$ is very unlike that of $pp \rightarrow \Delta^+ p$. We have no Coulomb singularity as $t \rightarrow 0$, and, from Fig. A2b we see that the Coulomb cross-section is only a factor of 3 larger than the strong cross-section, for $-t \approx 0.05$. Moreover, the γ-ray is now exchanged within nuclear force ranges. Thus we expect that the Coulomb process is strongly affected by absorption, and cannot simply be calculated from a one photon exchange diagram, as was done for Fig. A2b. We expect an interesting structure due to the Pomeron exchange, for example, which is then followed by a photon exchange. Furthermore, it is clear that we might expect large interference effects between the one-photon exchange diagrams and those with $\rho + A_2$ exchange. In order to extract the Δ(1238), it is clear that we must also measure $pp \rightarrow N^{*+}N^{*+}$, which will proceed by double diffraction dissociation, i.e. we must measure the mass spectrum of $p\pi^0$ events, and attempt to extract the Δ events. However, one will be measuring the rates of double diffractive dissociation, as a function of t and M^2, a problem very interesting in its own right in studying Pomeron exchange.

To do this without interfering with the R603 set-up, we propose to detect $p\pi^0$ modes, with one proton in the magnetic spectrometer, and one in the calorimeter. The magnet aperture is sufficiently large for us to place π^0 detectors behind it, so that one Δ^+ is detected in the magnetic spectrometer cum π^0 detector, and the other in the calorimeter cum π^0 detector arm. The trigger is: counts in both π^0 detectors, one charged particle in each arm, vetoes at the large angles, and large energy deposition in the calorimeter. Again, rates should be reasonable. Estimating a total $\Delta^+\Delta^+$ cross-section of ~ 0.3 μb, the number of these events is

$$R_{\Delta^+\Delta^+} = 0.1 \times 3 \times 10^{-31} \times \frac{2}{3} \times \frac{2}{3} \times 4 \times 10^{30}/\text{sec} \approx 50 \text{ counts/hour} .$$

The total number of diffractive events is probably at least an order of magnitude higher, with a different t-dependence.

3. SUMMARY

The physics proposed is to study the quasi-two-body reactions

$$pp \to \Delta^{++}\Delta^0 \quad (1)$$
$$pp \to \Delta^{++}n \quad (2)$$
$$pp \to \Delta^+\Delta^+ \quad (3)$$
$$pp \to \Delta^+p \quad (4)$$
$$pp \to N^{*+}N^{*+} \quad (5)$$
$$pp \to N^{*+}p \quad (6)$$

The first two reactions study $\rho + A_2$ exchange. Reactions (3) and (4) have dominant Coulomb contributions. Reactions (5) and (6) study low mass double diffraction dissociation and single diffraction dissociation, respectively, and are necessarily experimentally intertwined with (3) and (4). We propose to use the R603 apparatus in a compatible mode, i.e. without disturbing the physics scheduled for it, by adding to the detector capability. Specifically, we ask permission to add on the opposite arm a hadron calorimeter, MWPC, and π^0 detectors, as well as placing π^0 detectors behind the present magnet spectrometer. The expected counting rates for the various reactions are:

$R_1 \sim 150$ counts/h

$R_2 \sim 50$ counts/h

$R_3 \sim 10{,}000$ counts/h

$R_4 \sim 50$ counts/h

R_5 and R_6 unknown, but expected to be large.

The above rates were calculated for 1500 GeV. We expect in the VHE region that the charge exchange reactions go roughly as $1/s$, not $1/s^2$, and the counting rates R_1 and R_2 would be proportionally higher at the lower end of the ISR energy range. The Coulomb rate R_3 is expected to go as $\ln s$, and thus varies slowly. However, the acceptance for $t \approx 0$ Δ^+ decays improves markedly as we go to lower energies. Thus the experiments are easier at the lower end of the ISR energy spectrum.

We request 300 hours of running time and 200 hours of set-up time for this work, in its one-arm, asymmetric phase, over the ISR energy range. We feel that we would like the experience of this run before proposing moving to the symmetrical configuration of the R602 set-up. In the symmetric phase, calorimeters would be added to magnets on <u>both</u> arms, giving us identical experimental detection systems on both arms.

APPENDIX 1

THE THEORETICAL SITUATION

A1. General hypotheses

For VHE, we make the following simplifying assumptions for reactions (1) and (2):

i) π exchange is negligible relative to $\rho + A_2$;

ii) the $\rho + A_2$ have "Stodolsky-Sakurai Couplings", i.e. they always flip s-channel helicity one unit at the N-Δ vertex, and the size of the coupling for the helicity transitions $\frac{1}{2} \to -\frac{1}{2}$ is $1/\sqrt{3}$ the size for the transitions $\frac{1}{2} \to \frac{3}{2}$.

iii) a reasonable absorption model is utilized.

Because of assumptions (i) and (ii), the theoretical situation is rather simple, giving rise to many zeroes in the density matrix elements and very few amplitudes.

A2. $pp \to \Delta^{++}n$

For the above assumptions, there are three s-channel helicity state amplitudes needed to describe $pp \to \Delta^{++}n$. By analogy with NN scattering, we call them

a) M_5, which corresponds to <u>non-flip</u> at the pn vertex, <u>flip</u> at the NΔ vertex, and thus, a <u>net</u> flip of <u>one</u> unit;

b) M_2, which corresponds to <u>flip</u> at <u>both</u> vertices, but with a <u>net</u> flip of zero units;

c) M_4, which corresponds to flip at <u>both</u> vertices, but with a <u>net</u> flip of <u>two</u> units.

Letting <u>n</u> be the net helicity flip, the amplitudes M_4 and M_5, which have $n > 0$, have to vanish by angular momentum conservation as $t \to 0$, as $(-t)^{n/2}$, and they have no special structure.

On the contrary, we expect M_2 to have structure, a situation reminiscent of the conventional pion exchange case, responsible for the sharp

peaks in $np \to pn$, $\gamma p \to \pi^+ n$, etc. In the absence of absorption, however, even though M_2 has $n = 0$, it vanishes at $t \to 0$, because parity puts it equal to M_4. The situation is sketched below:

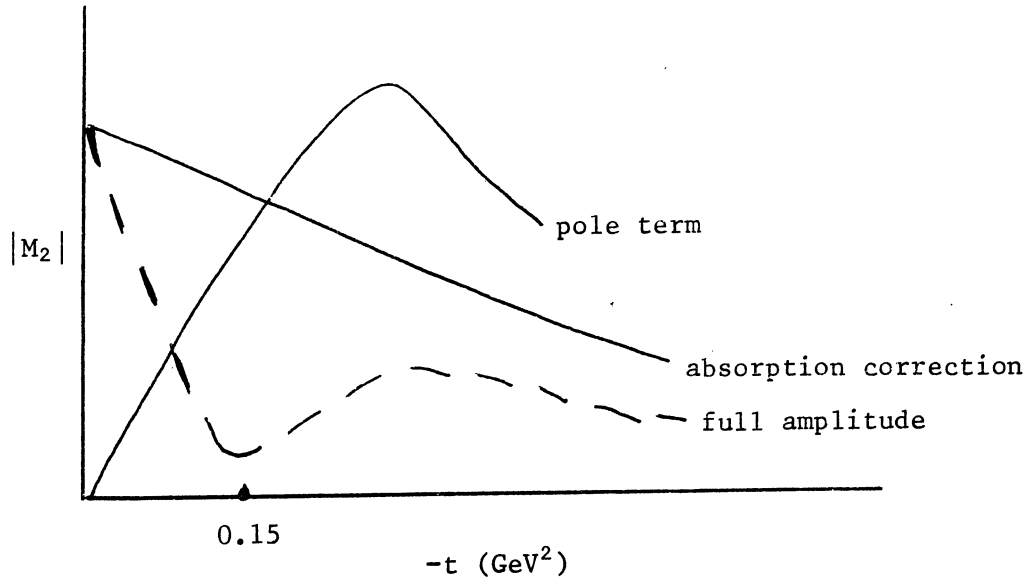

The solid curve labelled "pole" term is the pure pole contribution, before absorption. The curve labelled "absorption correction" is slowly varying in t, corresponding to a "cut", but is approximately out of phase with the "pole" contribution. The full amplitude is the dotted curve, which has a complex zero in the t-range $0.05 < -t < 0.1$ GeV^2. In the VHE region the t-structure is contained in M_2.

Defining $N = \frac{8}{3}\,(|M_2|^2 + |M_4|^2 + 2|M_5|^2)$, we can write

$$\frac{d\sigma}{dt} = \frac{389}{256q^2 s}\, N(\mu b/GeV^2)\ ,$$

with density matrix elements for the decay $\Delta^{++} \to \pi^+ p$, of $\rho_{33} = \frac{3}{8}$, $\rho_{11} = \frac{1}{8}$, $\rho_{31} = 0$, and

$$\text{Re}\ \rho_{3-1} = \frac{2}{\sqrt{3}}\left(\frac{|M_5|^2 + \text{Re}\ M_2 M_4^*}{N}\right)$$

$$\rho_{33} - \sqrt{3}\ \text{Re}\ \rho_{3-1} = \frac{|M_2 - M_4|^2}{N}\ .$$

The decay angular distribution $W(\theta,\phi)$ is given by:

$$W(\theta,\phi) = \frac{3}{4\pi}\left[\rho_{33}\sin^2\theta + \rho_{11}\left(\frac{1}{3} + \cos^2\theta\right) - \frac{2}{\sqrt{3}}\,\mathrm{Re}\,\rho_{3-1}\sin^2\theta\cos 2\phi - \right.$$

$$\left. - \frac{2}{\sqrt{3}}\,\mathrm{Re}\,\rho_{31}\sin 2\theta\cos\phi\right],$$

where all the ρ's are functions of s and t.

We note that by measuring the combination $\rho_{33} - \sqrt{3}\,\mathrm{Re}\,\rho_{3-1}$, we examine the sturcture <u>without</u> the presence of M_5. We further note that in a model <u>without</u> absorption,

$$\mathrm{Re}\,\rho_{3-1} = \sqrt{\frac{3}{8}} \quad \text{and} \quad \rho_{33} - \sqrt{3}\,\mathrm{Re}\,\rho_{3-1} = 0\ .$$

Figure A1a plots $d\sigma/dt$ versus t at 1500 GeV. Also shown are the individual contributions of $2|M_5|^2$ and $(|M_2|^2 + |M_4|^2)$. More detailed theoretical calculations are currently being made, using a computer program and estimating pion contributions, as well as being more accurate in the absorption estimates. The present theoretical results are probably no more accurate than a factor of 2.

The integrated cross-section of Fig. A1a is ~ 0.2 μb. This is to be compared with the extrapolated LHE cross-section (a^1/p^2 extrapolation), which gives ~ 0.025 μb.

Measurements of the density matrix elements ρ_{33}, ρ_{31}, and Re ρ_{31} will allow us to confirm assumptions (i) and (ii). The absorption model is tested by $\rho_{33} - \sqrt{3}\,\mathrm{Re}\,\rho_{3-1}$, and Re ρ_{3-1}.

A3. <u>$pp \to \Delta^{++}\Delta^0$</u>

This reaction is simpler than the previous one. Since we demand helicity flip at each vertex, there are only two amplitudes, corresponding to net helicity flip n = 0 or 2, which, by analogy to NN scattering, we call M_2 and M_4, respectively. The cross-section is given by

$$\frac{d\sigma}{dt} = \frac{389}{256q^2s}\,N\ \mu b/GeV^2\ ,$$

where $N = 32(|M_2|^2 + |M_4|^2)$.

We have a richer experimental situation, in that we can measure the joint decay density matrix of <u>both</u> Δ decays. In Section A6, we tabulate the decay distribution, which consists of 20 indepent measurable terms:

$$W(\theta_1,\phi_1;\ \theta_2,\phi_2) = \frac{9}{32\pi^2}\sum_{i=1}^{20} W_i(\theta_1,\phi_1;\ \theta_2,\phi_2)\ .$$

The density matrix consists of 256 elements, of which 72 are independent. Of these 72, 32 have no contribution to the decay distribution, and the remaining 40 group into pairs of 2, giving 20 measurables.

We employ the notation for the joint density matrix of $\rho^{NN'}_{MM'}$, where the Δ^{++} decays are labelled by M,M′ and the Δ^0 decays are labelled by N,N′. In our notation, the density matrix elements for the Δ^{++} <u>alone</u>, i.e. integrated over all decay configurations of the Δ^0, are given by $\rho_{MM'} = \sum_N \rho^{NN}_{MM'}$. Our model predicts the following, where we define $\alpha = 2M_2M_4^*/(|M_2|^2 + |M_4|^2)$ and $\beta = |M_2|^2/(|M_2|^2 + |M_4|^2)$:

$$\text{Re}\ \rho^{33}_{31} + \text{Re}\ \rho^{-3-3}_{31} = 0 \tag{A1}$$

$$\text{Re}\ \rho^{31}_{33} + \text{Re}\ \rho^{31}_{-3-3} = 0 \tag{A2}$$

$$\text{Re}\ \rho^{11}_{31} + \text{Re}\ \rho^{-1-1}_{31} = 0 \tag{A3}$$

$$\text{Re}\ \rho^{31}_{11} + \text{Re}\ \rho^{31}_{-1-1} = 0 \tag{A4}$$

$$\text{Re}\ \rho^{33}_{33} + \text{Re}\ \rho^{33}_{-3-3} = 9/32 \tag{A5}$$

$$\text{Re}\ \rho^{11}_{11} + \text{Re}\ \rho^{11}_{-1-1} = 1/32 \tag{A6}$$

$$\text{Re}\ \rho^{33}_{3-1} + \text{Re}\ \rho^{-3-3}_{3-1} = \frac{3\sqrt{3}}{8}\ \text{Re}\ \alpha \tag{A7}$$

$$\text{Re}\ \rho^{3-1}_{33} + \text{Re}\ \rho^{3-1}_{-3-3} = \frac{3\sqrt{3}}{8}\ \text{Re}\ \alpha \tag{A8}$$

$$\text{Re}\ \rho^{3-1}_{11} + \text{Re}\ \rho^{3-1}_{-1-1} = \frac{\sqrt{3}}{8}\ \text{Re}\ \alpha \tag{A9}$$

$$\text{Re}\ \rho^{3-1}_{11} + \text{Re}\ \rho^{3-1}_{-1-1} = \frac{\sqrt{3}}{8}\ \text{Re}\ \alpha \tag{A10}$$

$$\text{Re}\ \rho^{33}_{11} + \text{Re}\ \rho^{33}_{-1-1} = 3/32 \tag{A11}$$

$$\text{Re}\ \rho^{11}_{33} + \text{Re}\ \rho^{-1-1}_{33} = 3/32 \tag{A12}$$

$$\text{Re}\ \rho^{31}_{31} - \text{Re}\ \rho^{31}_{-1-3} = 0 \tag{A13}$$

$$\text{Re } \rho_{13}^{31} - \text{Re } \rho_{-31}^{13} = 0 \tag{A14}$$

$$\text{Re } \rho_{3-1}^{31} + \text{Re } \rho_{-31}^{13} = 0 \tag{A15}$$

$$\text{Re } \rho_{31}^{3-1} + \text{Re } \rho_{13}^{-31} = 0 \tag{A16}$$

$$\text{Re } \rho_{3-1}^{13} + \text{Re } \rho_{-31}^{31} = 0 \tag{A17}$$

$$\text{Re } \rho_{13}^{3-1} + \text{Re } \rho_{31}^{-31} = 0 \tag{A18}$$

$$\text{Re } \rho_{3-1}^{3-1} + \text{Re } \rho_{1-3}^{3-1} = 3/16\ \beta \tag{A19}$$

$$\text{Re } \rho_{-13}^{3-1} + \text{Re } \rho_{-31}^{3-1} = 3/16\ (1 - \beta)\,. \tag{A20}$$

If we integrate over one of the two delta decay distributions, we get

$$\rho_{11} = \rho^{11} = 1/8 \tag{A21}$$

$$\rho_{33} = \rho^{33} = 3/8 \tag{A22}$$

$$\text{Re } \rho_{31} = \text{Re } \rho^{31} = 0 \tag{A23}$$

$$\text{Re } \rho_{3-1} = \text{Re } \rho^{3-1} = \frac{\sqrt{3}}{2} \text{Re } \alpha\,. \tag{A24}$$

From the above, we note that we have a overabundance of correlations to determine the two parameters Re α and β.

In Fig. A1b, we plot $d\sigma/dt$ versus t for 1500 GeV, and also indicate the contributions separately of $|M_2|^2$, which contain all the structure.

The t-dependence is noticeably different from the reaction $pp \to \Delta^{++}n$, whereas the total cross-section is quite similar. We obtain an integrated cross-section of ~ 0.1 μb, a contribution about 5 times greater than the value estimated for pion exchange, obtained by extrapolation of $1/p^2$.

A4. $pp \to \Delta^+ p$

Charge independence relates the strong interaction processes $pp \to \Delta^+ p$ and $pp \to \Delta^{++}n$ by $\sigma(pp \to \Delta^+ p) = (\frac{1}{3})\sigma(pp \to \Delta^{++}n)$. However, as first pointed out by Nicol and Salin[2], there exists a competing electromagnetic process, which they calculated from the one-photon exchange graph

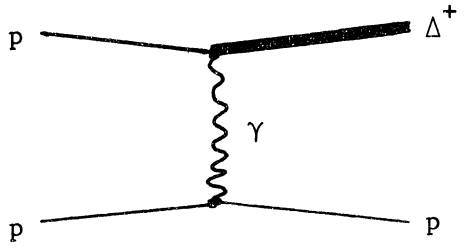

This process is rather singular in t, behaving as $d\sigma/dt \propto |t - t_0|/t^2$, where t_0 is the minimum squared four-momentum transfer; $t_0 = [(M_\Delta{}^2 - m_p{}^2)/2p_{lab}]^2$, where M_Δ = Δ mass, m_p = nucleon mass, and p_{lab} is the laboratory energy of the incoming proton, in the frame where the target proton is at rest. For 1500 GeV, $t_0 \approx 0.3 \times 10^{-7}$ GeV^2. Thus, one would effectively see a spike around t = 0 due to this cross-section, which, for $t >> t_0$, goes as $d\sigma/dt \propto 1/t$. Thus it is a singular cross-section, but somewhat less singular than the ordinary Coulomb cross-section for elastic scattering which goes as $1/t^2$. To illustrate the expected magnitude of the photon exchange and strong contribution, we plot the results of Ref. 2, along with the charge independence (strong interaction) prediction, in Fig. A2a. The Coulomb process obviously dominates for $|t| < 0.4$ GeV^2, being an order of magnitude layer for $|t| \sim 0.1$ GeV^2. It has been suggested by Gobbi and Rosen[3] that this calculable, one-photon exchange diagram, which dominates the low t region (because of the 1/t singularity) be used to make an absolute measure of the luminosity of ISABELLE. Indeed, the scheme seems practical for use at the ISR, where we use the sharp t-spike to separate the $\Delta(1236)$ from the background of diffractively produced $N^{*+} \to p\pi^0$. Scaling Gobbi and Rosen's numbers for 1500 GeV, we find that if only momentum transfers less than 30 MeV/c are measured, the integrated cross-section is 5 μb.

A5. $pp \to \Delta^+\Delta^+$

Charge independence relates the strong interaction processes $pp \to \Delta^{++}\Delta^0$ and $pp \to \Delta^+\Delta^+$ by $\sigma(pp \to \Delta^{++}\Delta^0) = (3/4)\sigma(pp \to \Delta^+\Delta^+)$. In the one-photon approximation,

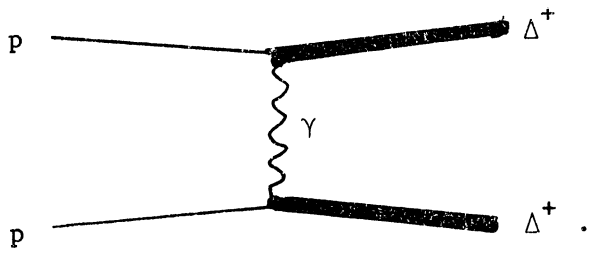

Nicot and Salin[2] have calculated the differential cross-section, which has been plotted in Fig. A2b, compared to the purely nuclear prediction of $\rho + A_2$ exchange. We see that for $|t| < 0.15$ GeV^2, the Coulomb process is ~ 3 times larger. We comment that this is a rather unique type of

Coulomb process, in that there is no inherent $1/t$ or $1/t^2$ dependence, i.e. no singularity at small t because of photon exchange, due to the dipole nature of the transition at each vertex. This implies that the photon is exchanged when the two protons are within nuclear force ranges, unlike the situation in $pp \to pp$ or $pp \to \Delta^+ p$ (by means of photon exchange) where the photon is exchanged at very large distances compared to nuclear force ranges. This type of γ-ray process will allow us to study the nuclear effects due to Pomeron exchange, etc., that take place between the two protons (which are now within a strong interaction range of each other) before the photon is exchanged, e.g.

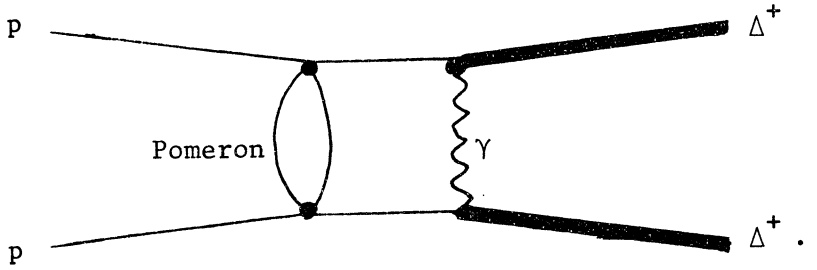

In other words, we will be using the photon as a probe to study absorption phenomena. Kane et al. are currently calculating the expected cross-section for γ-ray exchange along with absorption.

A6. Tabulation of the angular distribution in $pp \to \Delta^{++}\Delta^0$, $\Delta^+\Delta^+$

The double-decay angular distribution is given by $W(\theta_1,\phi_1;\ \theta_2,\phi_2) = W(\Omega_1;\ \Omega_2)$.

We write

$$W(\Omega_1;\ \Omega_2) = \frac{9}{32\pi^2} \sum_{i=1}^{20} W_i(\Omega_1;\ \Omega_2)$$

$$W_1 = -\frac{2}{\sqrt{3}} \left(\mathrm{Re}\ \rho_{31}^{33} + \mathrm{Re}\ \rho_{31}^{-3-3} \right) \sin 2\theta_1 \cos \phi_1 \sin^2 \theta_2$$

$$W_2 = -\frac{2}{\sqrt{3}} \left(\mathrm{Re}\ \rho_{33}^{31} + \mathrm{Re}\ \rho_{-3-3}^{31} \right) \sin^2 \theta_1 \sin 2\theta_2 \cos \phi_2$$

$$W_3 = -\frac{2}{\sqrt{3}} \left(\mathrm{Re}\ \rho_{31}^{11} + \mathrm{Re}\ \rho_{31}^{-1-1} \right) \sin 2\theta_1 \cos \phi_1 \left(\frac{1}{3} + \cos^2 \theta_1 \right)$$

$$W_4 = -\frac{2}{\sqrt{3}}\left(\mathrm{Re}\,\rho_{11}^{31} + \mathrm{Re}\,\rho_{-1-1}^{31}\right)\left(\frac{1}{3} + \cos^2\theta_1\right)\sin 2\theta_2 \cos\phi_2$$

$$W_5 = \left(\mathrm{Re}\,\rho_{33}^{33} + \mathrm{Re}\,\rho_{-3-3}^{33}\right)\sin^2\theta_1 \sin^2\theta_2$$

$$W_6 = \left(\mathrm{Re}\,\rho_{11}^{11} + \mathrm{Re}\,\rho_{-1-1}^{11}\right)\left(\frac{1}{3} + \cos^2\theta_1\right)\left(\frac{1}{3} + \cos^2\theta_2\right)$$

$$W_7 = -\frac{2}{\sqrt{3}}\left(\mathrm{Re}\,\rho_{3-1}^{33} + \mathrm{Re}\,\rho_{3-1}^{-3-3}\right)\sin^2\theta_1 \cos 2\phi_1 \sin^2\theta_2$$

$$W_8 = -\frac{2}{\sqrt{3}}\left(\mathrm{Re}\,\rho_{33}^{3-1} + \mathrm{Re}\,\rho_{-3-3}^{3-1}\right)\sin^2\theta_1 \sin^2\theta_2 \cos 2\phi_2$$

$$W_9 = -\frac{2}{\sqrt{3}}\left(\mathrm{Re}\,\rho_{3-1}^{11} + \mathrm{Re}\,\rho_{3-1}^{-1-1}\right)\sin^2\theta_1 \cos 2\phi_1 \left(\frac{1}{3} + \cos^2\theta_2\right)$$

$$W_{10} = -\frac{2}{\sqrt{3}}\left(\mathrm{Re}\,\rho_{11}^{3-1} + \mathrm{Re}\,\rho_{-1-1}^{3-1}\right)\left(\frac{1}{3} + \cos^2\theta_1\right)\sin^2\theta_2 \cos 2\phi_2$$

$$W_{11} = \left(\mathrm{Re}\,\rho_{11}^{33} + \mathrm{Re}\,\rho_{-1-1}^{33}\right)\left(\frac{1}{3} + \cos^2\theta_1\right)\sin^2\theta_2$$

$$W_{12} = \left(\mathrm{Re}\,\rho_{33}^{11} + \mathrm{Re}\,\rho_{33}^{-1-1}\right)\sin^2\theta_1 \left(\frac{1}{3} + \cos^2\theta_2\right)$$

$$W_{13} = \frac{2}{3}\left(\mathrm{Re}\,\rho_{31}^{31} - \mathrm{Re}\,\rho_{-1-3}^{31}\right)\cos(\phi_1 + \phi_2)\sin 2\theta_1 \sin 2\theta_2$$

$$W_{14} = \frac{2}{3}\left(\mathrm{Re}\,\rho_{13}^{31} - \mathrm{Re}\,\rho_{-3-1}^{31}\right)\cos(\phi_1 - \phi_2)\sin 2\theta_1 \sin 2\theta_2$$

$$W_{15} = \frac{2}{3}\left(\mathrm{Re}\,\rho_{3-1}^{31} + \mathrm{Re}\,\rho_{-31}^{13}\right)\cos(2\phi_1 + \phi_2)\sin^2\theta_1 \sin 2\theta_2$$

$$W_{16} = \frac{2}{3}\left(\mathrm{Re}\,\rho_{31}^{3-1} + \mathrm{Re}\,\rho_{13}^{-31}\right)\cos(\phi_1 + 2\phi_2)\sin 2\theta_1 \sin^2\theta_2$$

$$W_{17} = \frac{2}{3}\left(\mathrm{Re}\,\rho_{3-1}^{13} + \mathrm{Re}\,\rho_{-31}^{31}\right)\cos(2\phi_1 - \phi_2)\sin^2\theta_1 \sin 2\theta_2$$

$$W_{18} = \frac{2}{3}\left(\mathrm{Re}\,\rho_{13}^{3-1} + \mathrm{Re}\,\rho_{31}^{-31}\right)\cos(2\phi_2 - \phi_1)\sin 2\theta_1 \sin^2\theta_2$$

$$W_{19} = \frac{2}{3}\left(\mathrm{Re}\,\rho_{3-1}^{3-1} + \mathrm{Re}\,\rho_{1-3}^{3-1}\right)\cos(2\phi_1 + 2\phi_2)\sin^2\theta_1 \sin^2\theta_2$$

$$W_{20} = \frac{2}{3}\left(\mathrm{Re}\,\rho_{-13}^{3-1} + \mathrm{Re}\,\rho_{-31}^{3-1}\right)\cos(2\phi_1 - 2\phi_2)\sin^2\theta_1 \sin^2\theta_2 .$$

REFERENCES

1) G. Kane, I. Drummond and M.M. Block, private communication (1973).

2) R. Nicot and P. Salin, Nuclear Phys. B38, 247 (1972).

3) B. Gobbi and J.L. Rosen, "A scheme for absolute calibration of ISABELLE luminosity", Summer Study Design Proposal for ISABELLE.

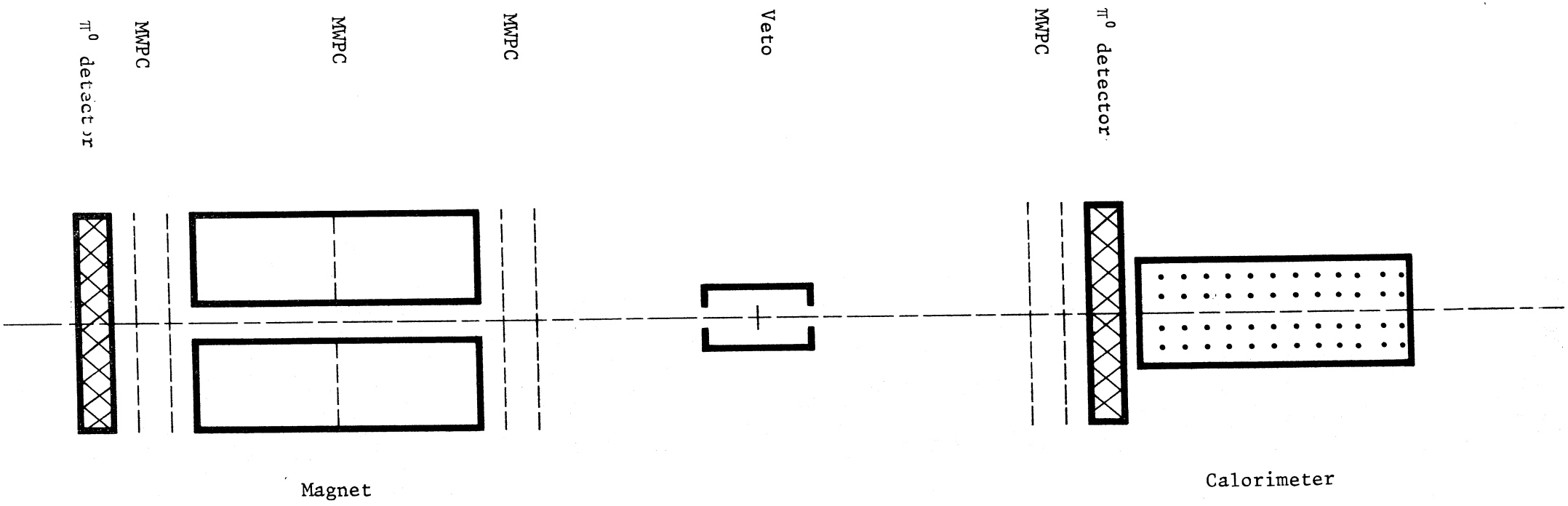

Fig. 1 Schematic of experimental layout

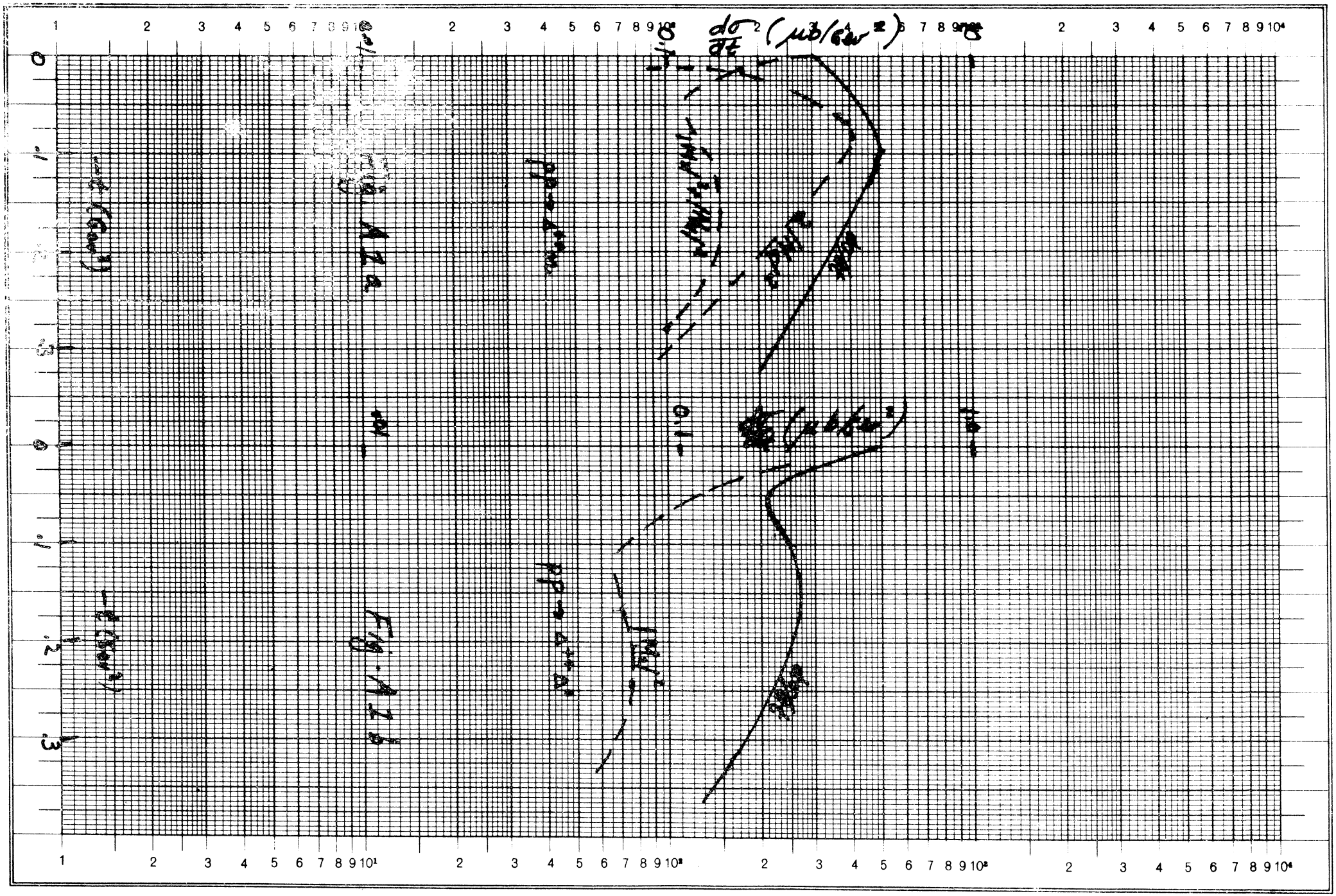

Logar. Teilung / Division 1-10000 Einheit / Unité 62,5 mm

Ed. Aerni-Lauch, Bern Nr. 826

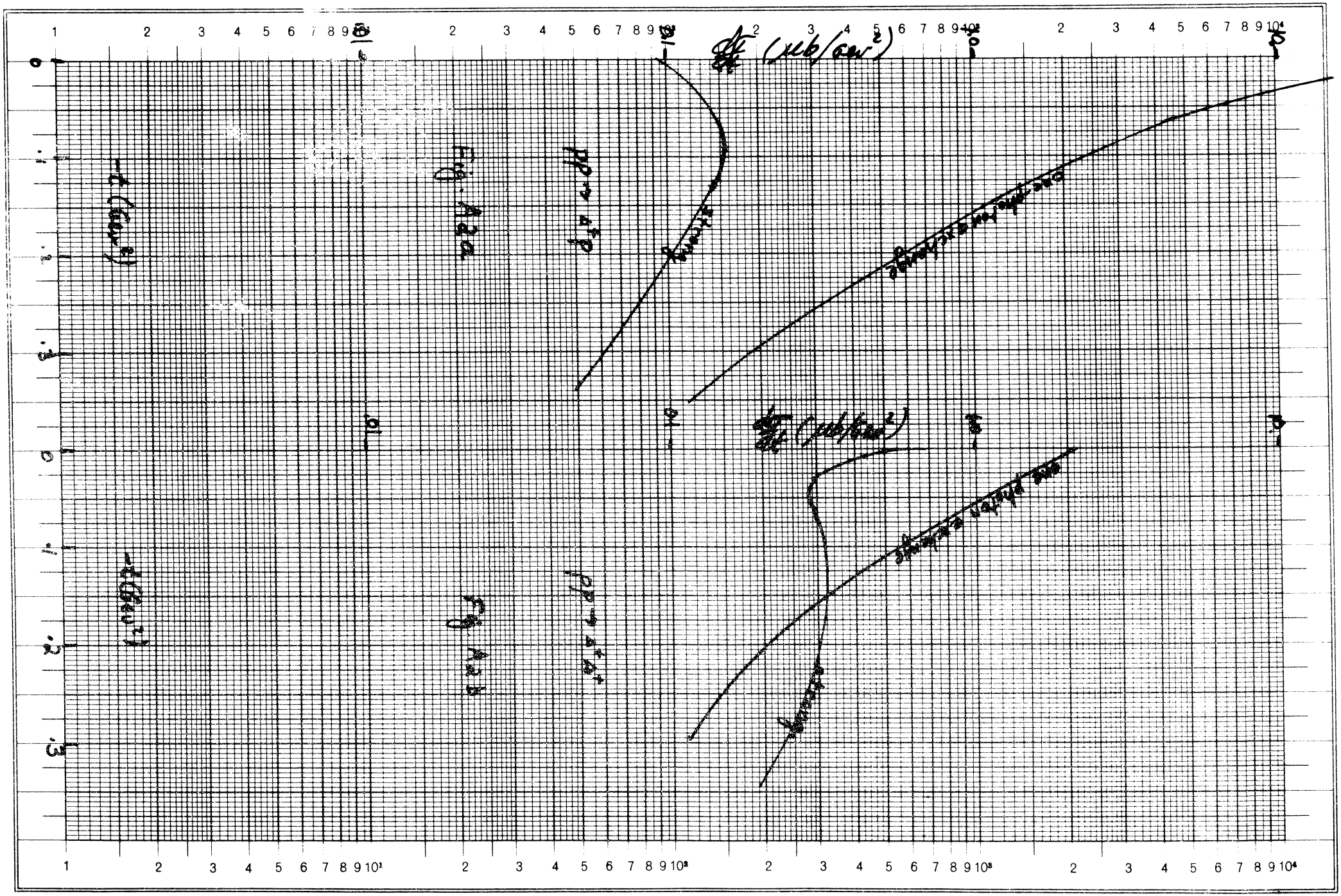

Logar. Teilung / Division } 1-10000 Einheit / Unité } 62,5 mm

Ed. Aerni-Leuch, Bern Nr. 526